Available online at www.sciencedirect.com
ScienceDirect
Journal of Nuclear Materials 367–370 (2007) 616–620
journal of nuclear materials
www.elsevier.com/locate/jnucmat

A critical stress–critical area statistical model of the $K_{J_c}(T)$ curve for MA957 in the cleavage transition

W.J. Yang [a,b], G.R. Odette [a,*], T. Yamamoto [a], P. Miao [a], M.J. Alinger [a], M. Hribernik [a], J.H. Lee [b]

[a] Department of Mechanical and Environmental Engineering, University of California, Santa Barbara, CA 93106-5050, United States
[b] Korea Institute of Machinery and Materials, 66, Sangnam-dong, Changwon-city, Kyeongnam 641-831, Republic of Korea

Abstract

We model the temperature (T) dependent fracture toughness $K_{J_c}(T)$ of MA957 based on a statistically modified critical stress–critical stressed area (σ^*–A^*) local fracture criteria. The $K_{J_c}(T)$ of MA957 is strongly dependent on the specimen orientation. Analysis of cleavage initiation in the longitudinal–radial (L–R) orientation, with the highest $K_{J_c}(T)$, yielded the highest $\sigma^* \approx 3600$ MPa. In contrast, the σ^* for the circumferential–longitudinal (C–L) orientation, with the lowest $K_{J_c}(T)$, yielded the lowest $\sigma^* \approx 2850$ MPa, while for the circumferential–radial (C–R) orientation with intermediate $K_{J_c}(T)$, $\sigma^* \approx 3000$ MPa. The A^* ranged from ≈ 30 to 400 μm^2. The cleavage initiation sites are μm-scale Al_2O_3 particles aligned in the textured low toughness extrusion direction.

1. Introduction

Iron–chromium based alloys, strengthened with a high number density of nm-scale yttrium–titanium–oxygen clusters (NCs) have demonstrated outstanding high temperature creep strength [1]. Mechanical alloying (MA) ferritic powders with Y_2O_3 and Ti by high-energy ball milling, followed by consolidation at elevated temperature produces nm-scale, Y–O–Ti features (NFs), as well as a more typical fine-to-coarser scale incoherent dispersed oxide particles [2,3]. We refer to these materials as nanostructured ferritic alloys (NFAs). The NFs are generally believed to be responsible for the high tensile and creep strength of NFAs. This high strength, coupled with high corrosion and radiation damage resistance, offers great promise for elevated temperature applications to fusion and advanced fission structures [4,5]. However, a challenge in the development of these alloys is maintaining adequate fracture toughness in combination with the high creep strength. Low toughness is a potential problem with these alloys since, in common with other BCC alloys, NFAs exhibit a ductile-to-brittle fracture mode transition over a characteristic range of temperature; and the very high strength of NFAs would be expected to result in decreased toughness relative to that of conventional steels. We have previously characterized the tensile and fracture toughness of as-hot extruded NFA MA957, showing that this alloy has highly

* Corresponding author. Tel.: +1 805 893 3525; fax: +1 805 893 8651.
E-mail address: odette@engineering.ucsb.edu (G.R. Odette).

0022-3115/$ - see front matter © 2007 Elsevier B.V. All rights reserved.
doi:10.1016/j.jnucmat.2007.03.203

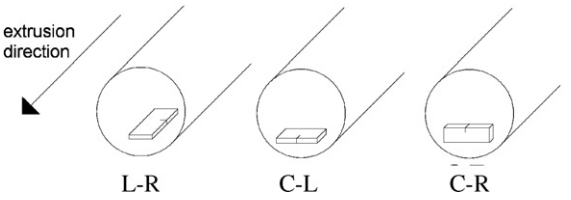

Fig. 1. The fracture specimen orientations referenced to the extrusion direction.

anisotropic properties and very low fracture toughness particularly in the circumferential–longitudinal (C–L) and circumferential–radial (C–R) orientations (see Fig. 1) [6]. MA957 is hot extruded at 1150 °C resulting in both elongated grains with a length to diameter ($\approx$ 0.5–1 μm) aspect ratio of $\approx$ 5 and crystallographic texturing. Further Al_2O_3 impurity inclusions are aligned as stringer particles in the extrusion direction. Thus a basic understanding of the micromechanical mechanisms controlling cleavage fracture, and how they relate to the underlying alloy structures, is critical to developing NFAs with adequate toughness. Three possible explanations for the anisotropy in the fracture properties and low toughness are proposed: (1) impurity alumina (Al_2O_3) particles from the ferrochrome powder source of the master alloy aligned in the extrusion direction provide geometrically favorable cleavage initiation sites; (2) the anisotropic grain size is effectively larger in the extrusion direction reducing the critical stress for microcracking; and (3) the high degree of [1 1 0] crystallographic texture imparted by hot extrusion produces an intrinsically brittle cleavage orientation.

2. Experimental procedures and FE stress field simulations

The fracture toughness and tensile data for MA957 were reported in an earlier publication [6]. Fracture tests were performed at various temperatures on pre-cracked $a/W \approx 0.5$, $W = B$ 1/3 Charpy sized ($3.33 \times 3.33 \times 18.33$ mm) bend bars in three orientations with respect to the extrusion direction shown in Fig. 1: L–R – longitudinal/length-radial crack plane; C–R – circumferential–transverse/length-radial crack plane; and C–L – circumferential–transverse/length longitudinal crack plane. The elastic and elastic–plastic $K_{J_c}(T)$ were evaluated in accordance with ASTM standard E1921 [7]. Cleavage fracture initiates by the rapid propagation of a cleavage microcrack from a broken brittle cleavage trigger particle in the highly stressed volume ahead of the crack tip. Microcrack propagation requires a local critical Griffith type stress that depends on: (a) the cracked particle size; (b) its orientation with respect to the adjacent ferrite grain; and (c) the corresponding orientation-dependent ferrite micro-crack arrest toughness. The cleavage trigger particles are statistically distributed in size and orientation; thus specimen-to-specimen sampling variations lead to intrinsic scatter in K_{J_c}. The greater the stressed volume, $V = BA(\sigma_{22})$, where A is the area enclosing a normal σ_{22} (to the crack plane) stress contour and B is the crack front length (specimen thickness), the higher the likelihood of activating a weakest link trigger particle leading to cleavage fracture. For this work, a modified critical stress–statistical stressed area (σ^*–A^*) concept was used to model $K_{J_c}(T)$ [8,9]. Plane strain 2D-FE calculations were used to simulate the stress distribution in front of a blunting semi-circular crack tip using the commercial ABAQUS code and the measured true stress–strain constitutive data fit to simple analytic functions. The quarter symmetry mesh was composed of 826 8-node isoparametric elements with a total of 2607 nodes. The mesh was highly refined at the crack tip with an initial radius to specimen with of 3.3×10^{-4} (1 μm). Post processing codes were used to evaluate $A(\sigma, T)$ for normal to yield stress ratios σ_{22}/σ_y from $\approx$ 2.4 to 3.6. Plots of $A(\sigma_{22}, T)$ versus σ_{22} were used to define σ^* for each orientation

3. Results

Fig. 2 shows the $A(\sigma_{22}, T)$ versus σ_{22}. Recognizing that the limited K_{J_c} data are statistically distributed, we defined σ^* at the point of the maximum number of intersections of the $A(\sigma,T)$ curves. Further we assumed that the spread in A^* at σ^* reflects the inherent statistical variations in the K_{J_c} data. The A^*–σ^* varied with orientation, as shown by the vertical lines in Fig. 2. In the L–R orientation (Fig. 2(a)) $\sigma^* \approx 3600$ MPa, while $\sigma^* \approx 2850$ MPa in the C–L orientation (Fig. 2(b)) and $\sigma^* \approx 3000$ MPa (Fig. 2(c)) in the C–R orientation. The A^* for the median toughness were similar, averaging 142 ± 10 μm^2 (see Table 1). The fracture toughness was found from $A(J = J_c) = A^*$ trajectories for each orientation.

The variation of the A^* and corresponding toughness can be crudely analyzed to specify the probability distribution of K_{J_c}. The cleavage fracture

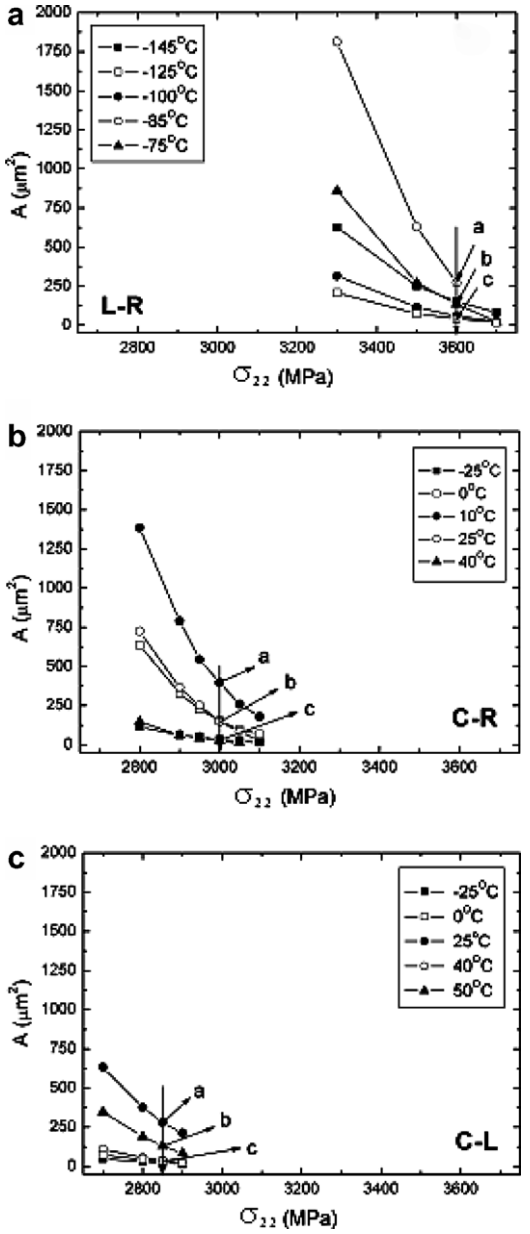

Fig. 2. The $A(\sigma, T)$ versus σ for each orientation and the points of maximum intersection defining σ^* (lines) for: (a) L–R; (b) C–R and (c) C–L.

Table 1
The local σ^* (MPa) and A^* (μm^2) for cleavage fracture properties for each orientation

	σ^* (MPa)	A^* for a	A^* for b	A^* for c
L–R	3600	270	144	49
C–R	3000	397	151	29
C–L	2850	281	132	30

probability, F, for a three-parameter Weibull distribution is:

$$F = 1 - \exp\left[-\left(\frac{K_{J_c} - K_{min}}{K_0 - K_{min}}\right)^4\right]. \quad (1)$$

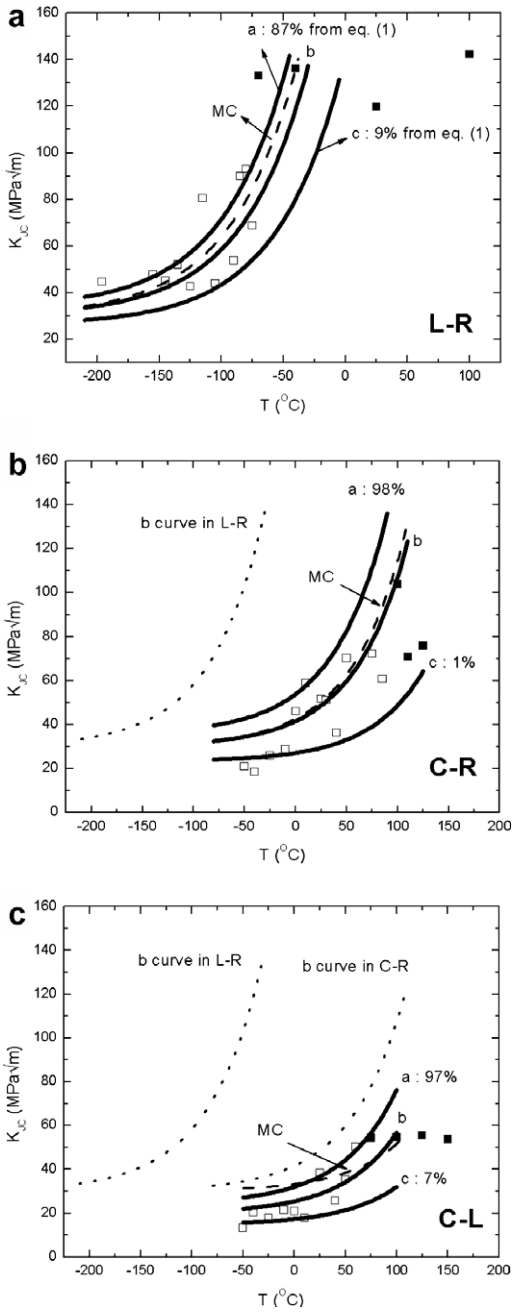

Fig. 3. Predicted $K_{J_c}(T)$ curves for the σ^*–A^* model for the median and specified fracture probability (F) conditions for the: (a) L–R; (b) C–R and (c) C–L orientations.

Here, K_{min} is the minimum fracture toughness, $m = 4$ is the Weibull toughness modulus, and K_0 is the K_J at $F = 0.632$. The points labeled a are for a high F, while those labeled c are for a low F. The intermediate points, labeled b, were taken as the nominal median value of K_{J_c} at $F = 0.5$. The values of σ^* and A^* for a, b and c and the various orientations are summarized in Table 1. The corresponding $K_{J_c}(T)$ curves cleavage for a, b and c are shown in Fig. 3 along with a master curve for comparison. As shown in Fig. 3(a), the data for the L–R orientation is consistent with $K_{min} = 20\ \mathrm{MPa}\sqrt{\mathrm{m}}$ with the high (a) and low (c) fracture probability curves falling at $F = 0.89$ and 0.09, respectively. A $K_{min} = 20\ \mathrm{MPa}\sqrt{\mathrm{m}}$ also provides a reasonable fit to the C–R data shown in Fig. 3(b), with the a and c points falling at $F = 0.98$ and 0.01, respectively. In both cases the predicted $K_{J_c}(T)$ are consistent with the master curve shape. However, fitting the C–L data (Fig. 3(c)) requires a lower $K_{min} = 10\ \mathrm{MPa}\sqrt{\mathrm{m}}$ with the a and c points falling at $F = 0.97$ and 0.07, respectively. These results suggest modified σ^*–A^* type models and the master curve (MC) concept can be applied to NFAs.

4. Discussion – the physical basis for anisotropic and low toughness orientations

The model-based analysis of the MA957 fracture data provides new insight regarding the challenges facing developing NFAs with adequate fracture toughness. We had previously argued that the low toughness in the C–L and, to a slightly lesser extent, in the C–R orientations was due to the stringers of impurity Al_2O_3 particles aligned in the extrusion direction. Thus if this were the sole reason for low toughness, the challenge would simply be to develop cleaner, inclusion free alloys. However, this explanation does not rationalize the high toughness in the L–R direction which, as illustrated in Fig. 4(a), is at least partially due to the tendency of the cracks to diverge out of the nominal ligament crack plane. This is in contrast to the planar cleavage fracture surfaces in the C–R and C–L orientations shown in Fig. 4(b) and (c). The torturous fracture path in the L–R orientation results in higher K_{J_c}, but the underlying reason for the out-of plane cracking is likely due to the existence of an easy cleavage system oriented for crack propagation in the extrusion direction due to texturing. Fig. 5 schematically illustrates the concept of crack propagation on the easy cleavage system, which is

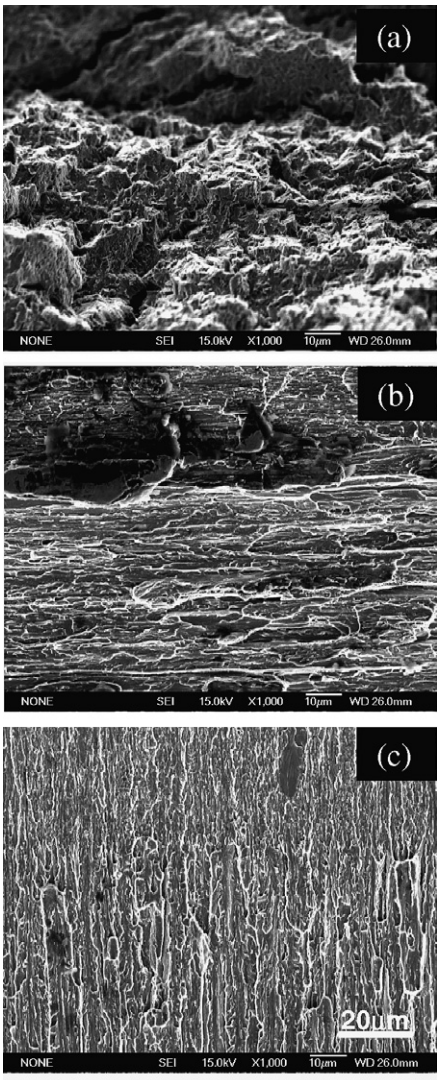

Fig. 4. Fracture surfaces for the: (a) L–R; (b) C–R; and (c) C–L orientations.

the (1 0 0) plane in [0 1 0] and [0 1 1] directions in ferrite, and trigger particle-effective grain size effects. The particle-stringer and elongated grain orientations are shown by the elliptical (C–R and C–L) and circular (L–R) shaped symbols. The easy cleavage plane is lightly shaded and the ligament fracture plane is shaded in deeper grey. Qualitatively, the larger particle and grain dimensions in the C–L orientation in the direction of crack propagation are expected to lead to the lowest σ^*. While the effective scale of the microstructure is smaller, the C–R orientation still has access to the easy cleavage system with an extrusion direction lying in the ligament plane, thus has an intermediate σ^*. However, in

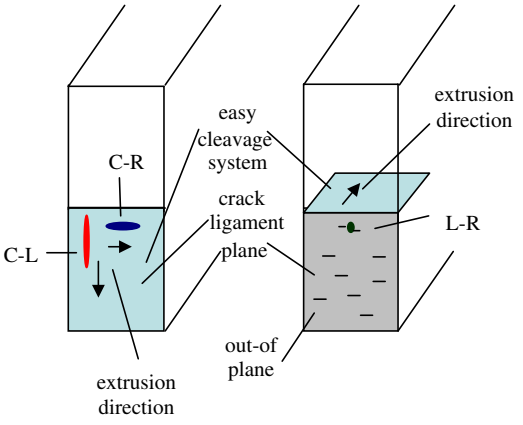

Fig. 5. Schematic illustration of possible mechanisms leading to the strong orientation dependence and low values of the C–R and the C–L K_{J_c}.

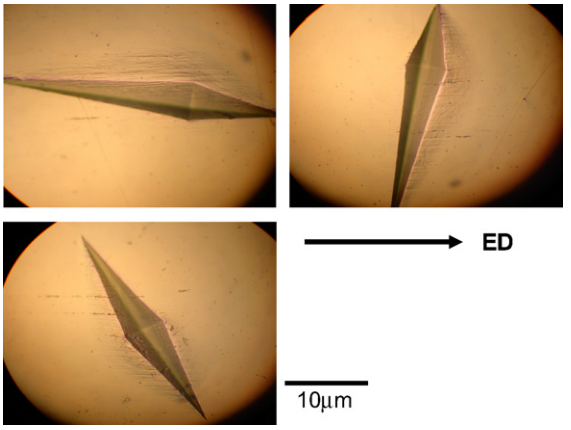

Fig. 6. Microcracks produced by various Knopp hardness indentations at −196 °C all propagating in the extrusion direction.

the L–R orientation the cracks must kink out of the ligament plane to access the easy cleavage system. In combination with the smallest effective microstructure size, this leads to the highest σ^*. As added support for the presence of easy cleavage systems, the strong tendency for indentation induced propagation of microcracks in the extrusion direction at 196 °C is shown in Fig. 6, independent of Knoop microhardness indenter orientation.

Acknowledgements

This research was supported by the DOE Office of Fusion Energy Science (Grant #DE-FG03-94ER54275) and the NERI DOE Office of Nuclear Energy (Grant #DE-FC07-05ID14663).

References

[1] S. Ukai, M. Harada, H. Okada, M. Inoue, S. Nomura, S. Shikakura, K. Asabe, T. Nishida, M. Fujiwara, J. Nucl. Mater. 204 (1993) 65.
[2] T. Okuda, M. Fujiwara, J. Mater. Sci. Lett. 14 (1995) 1600.
[3] M.J. Alinger, G.R. Odette, D.T. Hoelzer, J. Nucl. Mater. 329–333 (2004) 382.
[4] J.J. Fisher, US patent 4,075,010, Dispersion Strengthened Ferritic Alloy for use in Liquid Metal Fast Breeder Reactors, February 21, 1978.
[5] G.D. Smith, J.J. deBarbadillo, in: J.J. deBarbadillo et al. (Eds.), Structural Applications of Mechanical Alloying, ASM International, Materials Park, OH, 1994, p. 117.
[6] M.J. Alinger, G.R. Odette, G.E. Lucas, J. Nucl. Mater. 307–311 (2002) 484.
[7] E 1921 03 Annual Book of ASYM Standards 2004 V03.01, 2004, p. 1143.
[8] H.J. Rathbun, G.R. Odette, M.Y. He, T. Yamamoto, Eng. Fract. Mech. 73 (2006) 2723.
[9] G.R. Odette, T. Yamamoto, H.J. Rathbun, M.Y. He, M.L. Hribernik, J.W. Rensman, J. Nucl. Mater. 323 (2003) 313.